



**HAL**  
open science

## Real-Time Assessment of Myocardial Contractility Using Shear Wave Imaging

Mathieu Pernot, Mathieu Couade, Philippe Mateo, Bertrand Crozatier,  
Rodolphe Fischmeister, Mickaël Tanter

► **To cite this version:**

Mathieu Pernot, Mathieu Couade, Philippe Mateo, Bertrand Crozatier, Rodolphe Fischmeister, et al.. Real-Time Assessment of Myocardial Contractility Using Shear Wave Imaging. Journal of the American College of Cardiology, 2011, 58 (1), pp.65-72. 10.1016/j.jacc.2011.02.042 . hal-02940310

**HAL Id: hal-02940310**

**<https://hal.science/hal-02940310>**

Submitted on 16 Sep 2020

**HAL** is a multi-disciplinary open access archive for the deposit and dissemination of scientific research documents, whether they are published or not. The documents may come from teaching and research institutions in France or abroad, or from public or private research centers.

L'archive ouverte pluridisciplinaire **HAL**, est destinée au dépôt et à la diffusion de documents scientifiques de niveau recherche, publiés ou non, émanant des établissements d'enseignement et de recherche français ou étrangers, des laboratoires publics ou privés.

# Real-time Assessment of Myocardial Contractility using Shear Wave Imaging

Mathieu Pernot, PhD,<sup>\*,†,‡,§</sup> Mathieu Couade, MSc,<sup>\*,||</sup> Philippe Mateo, PhD,<sup>¶,#</sup> Bertrand Crozatier, MD, PhD,<sup>¶,#</sup> Rodolphe Fischmeister, PhD,<sup>¶,#</sup> Mickaël Tanter, PhD<sup>\*,†,‡,§</sup>

\*Institut Langevin, ESPCI ParisTech, Paris, 75005 France;

† CNRS, UMR 7587, Paris, 75005 France;

‡ INSERM, U979, Paris, 75005 France;

§ Université Paris Diderot-Paris7, Paris, 75013 France;

|| SuperSonic Imagine, Aix-en-Provence, 13857 France;

¶ INSERM, UMR-S 769, IFR141, Châtenay-Malabry, 92296 France;

# Université Paris-Sud, Faculté de Pharmacie, Châtenay-Malabry, 92296 France.

Short Title : Ultrasonic measurement of myocardial contractility.

Total word count : 2997

Corresponding address: [mathieu.pernot@espci.fr](mailto:mathieu.pernot@espci.fr)

Institut Langevin, ESPCI

10 rue Vauquelin, 75005 Paris, France

Tel: +33140794694

Fax: +33140794468

## **Abstract**

**Objectives** The goal of this study was to assess whether myocardial stiffness could be measured by Shear Wave Imaging (SWI) and whether myocardial stiffness accurately quantified myocardial function.

**Background** SWI is a novel ultrasound-based technique for quantitative, local and non-invasive mapping of soft tissues elastic properties.

**Methods** SWI was performed in Langendorff perfused isolated rat hearts (n=6). Shear wave was generated and imaged in left ventricular myocardium using a conventional ultrasonic probe connected to an ultrafast scanner (12,000 frames/s). The local myocardial stiffness was derived from shear wave velocity every 7.5 ms during one single cardiac cycle.

**Results** The average myocardial stiffness was  $8.6 \pm 0.7$  kPa in systole, and  $1.7 \pm 0.8$  kPa in diastole. Myocardial stiffness was compared with isovolumic systolic pressure at rest and during administration of isoproterenol ( $10^{-9}$ ,  $10^{-8}$  and  $10^{-7}$  M, 5 min each). Systolic myocardial stiffness increased strongly up to  $23.4 \pm 3.4$  kPa. Myocardial stiffness correlated strongly with isovolumic systolic pressure ( $r^2=[0.94;0.98]$ ,  $p < 0.0001$ ).

**Conclusions** Myocardial stiffness can be measured in real-time over the cardiac cycle using SWI which allows quantification of stiffness variation between systole and diastole. Systolic myocardial stiffness provides a non-invasive index of myocardial contractility.

**Keywords:** elasticity • echocardiography • contractility • imaging • myocardium

## **Abbreviation list**

SWI: Shear Wave Imaging

LV: Left Ventricle

## Introduction

Different indexes of ventricular contractility have been proposed (1,2) but most of them are either dependent on load conditions (3) or cannot be measured non invasively. The importance of ventricular stiffness has been shown through the powerful concept of time-varying elastance formalized by Suga and Sagawa (4) which provides a comprehensive description of the link between ventricular stiffness and cardiac function. However, despite the clinical importance of this concept, there is currently no non-invasive method for measuring the time-varying myocardial stiffness.

Two-dimensional echocardiography has become the imaging modality of choice for non invasive evaluation of regional myocardial function. New imaging modes such as tissue Doppler imaging (5) and strain or strain rate imaging (6) have been shown to provide good indicators for evaluation of abnormal LV function (7,8). However, myocardial strain imaging is highly load-dependent (8) and is therefore difficult to use as an index of myocardial contractility. Another method proposed by Hsu *et al.* (9) consists in inducing remotely a local strain in the myocardium using acoustic radiation force to assess myocardial stiffness under the assumption of uniform stress at the focus.

In this study, we propose a novel approach for measuring the local myocardial stiffness. Our method is based on shear wave imaging (SWI), an ultrasound-based technique for mapping quantitatively the stiffness of soft tissues characterized by the Young's modulus defined by the slope of the stress/strain curve (10). This technique belongs to the field of multiwave imaging as it combines two different waves: one (shear wave) providing stiffness contrast, another (ultrasound) providing millimeter spatial resolution (11). The clinical potential of this approach has been recently demonstrated in the field of breast lesions imaging (12), as well as in the liver (13), arteries (14) and for the monitoring of thermal ablation (15).

The first goal of this study was to demonstrate the feasibility of measuring the dynamics of myocardial stiffness with high temporal resolution and good reproducibility. The second goal was to

demonstrate that systolic stiffness can be used as an index of contractility by comparing it to conventional contractility indexes in normal heart.

## Methods

**Shear wave imaging.** SWI (10,16) is based on the remote generation of shear waves in soft tissue by the acoustic radiation force at the focus of an ultrasound field. A short duration burst (300  $\mu$ s) of focused ultrasound was transmitted by a diagnostic ultrasonic probe (linear array, 128 elements, 12 MHz central frequency, Vermon, France) to induce micrometric tissue displacements in a small zone of the myocardium thanks to the acoustic radiation force (Figure 1.a). This burst was composed of three transmits of 100  $\mu$ s focused successively at three focus separated by 2 mm in depth. In response to that transient mechanical excitation, a shear wave was generated in the low kHz frequency range and propagated in the myocardium at velocities between 1 and 10 m/s, depending on tissue stiffness (Figure 1.b). The originality of SWI consists in imaging the shear wave propagation at ultra-high frame rate (12,000 images/s) using the same diagnostic probe connected to an ultrafast ultrasonic scanner (Aixplorer<sup>TM</sup>, SuperSonic Imagine, France). The whole acquisition of the shear wave propagation was performed within 5 ms. The raw data were transferred to a computer and processed off-line. Tissue velocity maps were computed for each frame of the acquisition using IQ frame to frame cross-correlation. Myocardial wall motion was removed by subtraction of the average wall motion during the acquisition bringing to light tissue motion solely induced by the shear wave (Figure 1.c.d.e). Shear velocity was computed at each depth of the image using the spatio-temporal data of the shear wave propagation. Finally, the shear modulus  $\mu$  (i.e. stiffness) was derived at each location using the equation:

$$\mu = \rho c^2 \quad \text{Eq. 1}$$

where  $c$  is the shear velocity and  $\rho$  the volumic mass of the tissue. A time-of-flight algorithm described in a previous study (17) was used to derive a complete stiffness map in the region reached by the shear wave.

Forty stiffness measurements were repeated at high rate over two cardiac cycles to investigate myocardial stiffness dynamics. Each stiffness measurement was achieved within 5 ms and was repeated every 7.5 ms (acquisition repetition frequency of 133 Hz). The ventricular pressure was recorded at the same time on an external analog to digital board (Usbamp, gTec, Austria) allowing synchronization of the acquisition in post-treatment.

**Experimental setup.** SWI was performed in Langendorff perfused isolated adult rat hearts (Heart/body weight ratio:  $3.7 \pm 0.3$  mg/g,  $n=6$ ). The isolated hearts were immersed into a saline bath ( $50 \times 50 \times 50$  mm<sup>3</sup>) and the ultrasonic array was positioned through an acoustic window performed on the side of the water tank (Supplemental Fig. 1). In all experiments, the probe orientation was long axis view unless specified. The distance between the array and the heart was approximately 5 mm.

**Ex vivo physiology.** All experiments were carried out according to the European Community guiding principles in the care and use of animals (86/609/CEE). *Ex vivo* physiology experiments were performed in Langendorff perfused isolated rat hearts ( $n=6$ ) according to previously described methods (17) (Please see the supplemental methods section). Preload was modified by varying balloon volume by 5  $\mu$ L increment. Contractility was modified by changing Krebs extracellular  $\text{Ca}^{2+}$  concentrations or by infusing increasing concentrations of isoproterenol.

**Statistical analysis.** Changes in myocardial stiffness were analyzed using a paired two-tailed *t*-test to evaluate the significance of difference between individual mean values under different inotropic

effects or preload conditions. Linear regression was used for correlation between systolic stiffness and contractility. Statistical significance was inferred for  $p < 0.05$ . Values are presented as mean $\pm$ s.d.

## Results

**Myocardial stiffness mapping.** Figure 2.a shows a typical stiffness map obtained at one period of the cardiac cycle. The maps were computed in the region reached by the shear wave which was approximately 2 mm wide by 5 mm deep on each side of the pushing locations (see Figure 2.a). A small region of interest (ROI) of 1.4 mm (lateral) x 0.75 mm (depth) was chosen in the midwall region of the myocardium. In the following, myocardial stiffness was averaged in the ROI.

**Myocardial stiffness dynamics.** The variation of stiffness was measured with a good reproducibility in all animals. A typical time course of myocardial stiffness is shown in Figure 2.b: a sharp stiffening ( $d\mu/dt_{\max} = 163 \pm 21 \text{ kPa}\cdot\text{s}^{-1}$ ) is observed at the beginning of the systolic phase, reaches a maximum ( $\mu = 8.4 \pm 0.5 \text{ kPa}$ ) then decreases during end-systole and diastole, and finally returns to the initial state in the last part of the diastolic phase ( $\mu = 1.2 \pm 0.1 \text{ kPa}$ ). As shown in Figure 2.b, the shape of the time-varying stiffness was similar to the LV isovolumic pressure curve with stiffness peaks slightly preceding the pressure peaks. In this study, we define the diastolic and systolic stiffness as respectively the minimum and maximum values of myocardial stiffness during a cardiac cycle. Measurement reproducibility was assessed for 5 acquisitions in the same experimental conditions for each heart. As shown in Figure 2, a good reproducibility was found for diastolic stiffness (s.d. = 0.08 kPa), while the standard deviation of stiffness was 0.5 kPa in systole, which corresponded to a maximum error of  $\pm 6\%$ .

**Preload dependence of myocardial stiffness.** The variation of stiffness with preload was investigated by inflating progressively the latex water-filled balloon inserted into the LV. Figure 3 shows diastolic

and systolic myocardial stiffness as a function of LV systolic pressure in one control heart. Before inflation of the balloon, systolic pressure was  $77.1 \pm 5.9$  mmHg. The balloon was then progressively inflated by 5  $\mu$ L increment to a maximal volume of 70  $\mu$ L which increased systolic pressure to  $132.4 \pm 12.5$  mmHg due to Starling's law. Systolic myocardial stiffness was found to increase by ~20%, from  $10.1 \pm 0.6$  kPa to a maximum of  $12.3 \pm 0.7$  kPa ( $p < 0.005$ ). In contrast, diastolic stiffness did not change significantly with preload and was  $0.98 \pm 0.2$  kPa. Similar results were found in the six hearts (see Table 1). The average relative increase in systolic myocardial stiffness was  $26 \pm 4\%$ . These results show that myocardial stiffness is relatively independent of preload over a large range of pressure. The effect of heart rate was also investigated (Supplemental Fig. 3).

**Ca<sup>2+</sup> concentration dependence of myocardial stiffness.** Figure 4 shows myocardial stiffness as a function of Ca<sup>2+</sup> concentration in Ringer's solution. For each concentration, three LV volumes were investigated: the balloon was completely deflated (0  $\mu$ L), inflated to 10  $\mu$ L and finally to 25  $\mu$ L in order to study the dependence with preload. The increase in Ca<sup>2+</sup> concentration led to a strong increase in systolic stiffness, whereas the preload conditions did not change significantly the stiffness. Finally, diastolic stiffness did not vary significantly in any of these experiments.

**Myocardial stiffness during  $\beta$ -adrenergic stimulation.** The variation of myocardial stiffness during isoproterenol stimulation is shown as a function of time in Figure 5. Systolic stiffness increased immediately after stimulation and followed the evolution of systolic pressure. Figure 6 shows myocardial systolic stiffness response at different concentrations of isoproterenol ( $10^{-9}$ ,  $10^{-8}$  and  $10^{-7}$  M). Systolic stiffness was found to increase strongly upon administration of isoproterenol (up to  $23.4 \pm 3.4$  kPa) and followed a similar increase than  $(dp/dt)_{max}$ . Diastolic stiffness was unchanged in all hearts (not shown). The response of myocardial stiffness to isoproterenol was also evaluated in a LV hypertrophy model (Supplemental Figure 4).

To evaluate the efficacy of myocardial stiffness to reflect inotropic changes, systolic stiffness was compared to peak systolic pressure  $P_{\max}$  values. In isovolumic conditions such as in the Langendorff model,  $P_{\max}$  gives directly access to an approximation of the end-systolic pressure-volume relation which is a conventional index of contractility. Figure 7 shows the variation of systolic stiffness as a function of  $P_{\max}$  during isoproterenol stimulation in one heart. SWI was performed approximately every 20 seconds during 3 minutes to measure the change in stiffness during transitory response to isoproterenol stimulation. Myocardial stiffness appeared to be linearly related to  $P_{\max}$  in all hearts ( $0.94 < r^2 < 0.98$ ,  $p < 0.0001$ ). Table 2 shows a good reproducibility in the relationship between  $P_{\max}$  and stiffness on 6 hearts. A mean slope of  $0.22 \pm 0.2$  kPa/mmHg and a mean intercept of  $-8.8 \pm 0.3$  kPa were found.

## Discussion

In this study we have shown the feasibility of measuring myocardial stiffness locally and its dynamics over the cardiac cycle using SWI in Langendorff perfused rat hearts. Myocardial stiffness was measured with a good reproducibility (s.d.<6%). Peak systolic stiffness was found to be relatively independent of preload conditions but strongly dependent on inotropic state, as evidenced by the stimulatory effects of  $Ca^{2+}$  or a  $\beta$ -adrenergic agonist. A strong correlation was found between systolic myocardial stiffness and a reference contractility index. These results demonstrate that peak systolic myocardial stiffness has the potential to be used as an index of myocardial contractility.

Ideally, an index of contractility should only reflect the intrinsic contractile state of the myocardium, and therefore be independent of load conditions. The end-systolic elastance  $E_{es}$  has been shown to correctly describe the intrinsic contractile state, but its determination requires invasive catheterization for measurement of LV pressure. Therefore, a non invasive technique that would allow evaluation of the time-varying stiffness or elastance would be of great interest. In this paper we propose such a technique for local measurements of myocardial stiffness and its time-dependent variations. Similarly to end-systolic elastance, we have shown that end-systolic myocardial stiffness

was relatively load independent and could be used as an index of contractility. The theoretical relationship between Young's modulus and elastance has already been investigated by Sagawa et al. (18). In this study we provide an experimental demonstration of this relationship. Since SWI can measure quantitatively the local myocardial stiffness in a small region of the ventricle (of millimetric dimensions), this technique has the potential of providing a regional index of contractility. However, further investigations are required to demonstrate this regional capability.

Contrary to strain-based techniques, this method allows direct measurement of the local stress/strain relationship in myocardium (i.e. myocardial stiffness). In the field of soft tissue rheology, the assessment of stress/strain relationship of a biological tissue is necessary to fully characterize its intrinsic mechanical properties (19). This is even more important for cardiac applications, as myocardial stiffness provides important insights into the intrinsic mechanical properties of the beating heart. Myocardial stiffness is relatively independent of external stress and accurately reflects myocardial properties in their active or passive states. While previous attempts to estimate the regional elastance using strain imaging have failed due to the difficulty of measuring regional stress, our method may offer a novel tool for quantitative mapping of the regional elastance and myocardial contractility. Another advantage of this technique is its relative low sensitivity to motion artifacts thanks to the use of very high frame rates.

One limitation of our study is that it was performed *ex vivo*. The Langendorff setup offered stabilized experimental conditions which allowed us to investigate the link between systolic stiffness and contractility. However, as any more conventional ultrasonic-based techniques, SWI could be fully implemented *in vivo* for non-invasive imaging of the human heart and our efforts will focus in this direction. *In vivo* implementation will require the use of an ultrasonic probe dedicated to echocardiography with the correct choice of frequency and geometrical design for imaging through intercostal spaces. A lower imaging frequency (around 3 MHz), would be used for human heart imaging. We have already shown the technical feasibility of SWI *in vivo* in open-chest animals (20).

Another limitation is that local stiffness does not necessarily reflect the elastance and contractile function of the whole ventricle which may vary regionally. As shown in this study, SWI can be used to derive a map of the local myocardial elastic properties in the region where shear waves propagate. It is possible to extend this region to map the entire ventricle by generating additional shear waves at different locations. The stiffness mapping of the entire ventricle could have important clinical applications for the diagnostic of cardiac pathologies with important heterogeneities of myocardial elastic properties, such as regional ischemia or dilated cardiomyopathy. Diastolic dysfunctions may also benefit from this technique by quantifying myocardial diastolic stiffness.

## References

1. Little W. The left ventricular dP/dtmax-end-diastolic volume relation in closed- chest dogs. *Circ Res* 1985;56(6):808-815.
2. Sagawa K, Suga H, Shoukas AA, Bakalar KM. End-systolic pressure/volume ratio: a new index of ventricular contractility. *Am J Cardiol* 1977;40:748-753.
3. Su J, Crozatier B. Preload-induced curvilinearity of left ventricular end-systolic pressure-volume relations. Effects on derived indexes in closed-chest dogs. *Circulation* 1989;79:431-440.
4. Suga H, Sagawa K. Instantaneous Pressure-Volume Relationships and Their Ratio in the Excised, Supported Canine Left Ventricle. *Circ Res* 1974;35:117-126.
5. Sutherland GR, Stewart MJ, Groundstroem KW, et al. Color Doppler myocardial imaging: a new technique for the assessment of myocardial function. *J Am Soc Echocardiogr* 1994;7:441-458.

6. D'hooge J, Heimdal A, Jamal F, et al. Regional strain and strain rate measurements by cardiac ultrasound: principles, implementation and limitations. *Eur J Echocardiogr* 2000;1:154-170.
7. Edvardsen T, Skulstad H, Aakhus S, Urheim S, Ihlen H. Regional myocardial systolic function during acute myocardial ischemia assessed by strain Doppler echocardiography. *J Am Coll Cardiol*. 2001;37(3):726-30.
8. Voigt J, Lindenmeier G, Werner D, et al. Strain rate imaging for the assessment of preload-dependent changes in regional left ventricular diastolic longitudinal function. *J Am Soc Echocardiogr* 2002;15:13-19.
9. Hsu SJ, Bouchard RR, Dumont DM, Wolf PD, Trahey GE. In vivo assessment of myocardial stiffness with acoustic radiation force impulse imaging. *Ultrasound Med Biol* 2007;33:1706-1719.
10. Bercoff J, Tanter M, Fink M. Supersonic shear imaging: a new technique for soft tissue elasticity mapping. *IEEE Trans Ultrason Ferroelectr Freq Control* 2004;51:396-409.
11. Fink M, Tanter M. Multiwave imaging and super-resolution. *Phys Today* 2010;63:28.
12. Tanter M, Bercoff J, Athanasiou A, et al. Quantitative assessment of breast lesion viscoelasticity: initial clinical results using supersonic shear imaging. *Ultrasound Med Biol* 2008;34:1373-1386.
13. Muller M, Gennisson J, Deffieux T, Tanter M, Fink M. Quantitative viscoelasticity mapping of human liver using supersonic shear imaging: Preliminary in vivo feasibility study. *Ultrasound Med Biol* 2009;35:219-229.
14. Couade M, Pernot M, Prada C, et al. Quantitative assessment of arterial wall biomechanical

- properties using shear wave imaging. *Ultrasound Med Biol* 2010;36:1662-76.
15. Bercoff J, Pernot M, Tanter M, Fink M. Monitoring thermally-induced lesions with supersonic shear imaging. *Ultrasonic imaging* 2004;26:71-84
  16. Sarvazyan AP, Rudenko OV, Swanson SD, Fowlkes JB, Emelianov SY. Shear wave elasticity imaging: a new ultrasonic technology of medical diagnostics. *Ultrasound Med Biol* 1998;24:1419-35.
  17. Abi-Gerges A, Richter W, Lefebvre F, et al. Decreased expression and activity of cAMP phosphodiesterases in cardiac hypertrophy and its impact on  $\beta$ -adrenergic cAMP signals. *Circ Res* 2009;105:784-792.
  18. Sagawa K, Maughan L, Suga H, Sunagawa K. *Cardiac Contraction and the Pressure-Volume Relationship*, Oxford University Press, 1988.
  19. Fung, Y. *Biomechanics: mechanical properties of living tissues*. Springer, 1993.
  20. Couade M, Pernot M, Messas E et al. In vivo quantitative mapping of myocardium stiffening and transmural anisotropy using Supersonic Shear Imaging. *IEEE Trans Med Imaging* 2010 (in press).

## Figure legends

### Figure 1. SWI principle

a) Shear wave generation: an ultrasonic burst is focused into the myocardium. The acoustic radiation force generates tissue displacements on the order of 1  $\mu\text{m}$  at the focal zone. b) Ultrafast imaging: pulse plane waves are transmitted by the same ultrasonic probe at repetition frequency of 12,000 Hz. The pulse-echo signals are stored on a computer, images are beamformed offline. Tissue velocity maps obtained in a rat heart are computed and shown on figures c), d) and e), respectively 0.3 ms, 1.0 ms and 1.5 ms after inducing the shear wave.

### Figure 2. Myocardial stiffness dynamics

a) An example of myocardial stiffness map obtained in a rat heart in the region reached by the shear wave. The pushing locations are shown by three red dots. The region of interest where the shear wave velocity is calculated is shown by a white box. b) Myocardial stiffness variation within a cardiac cycle for a control heart (mean  $\pm$  s.d. of 5 different cardiac cycles). The mean LV pressure (continuous line)  $\pm$  s.d. (dotted lines) is plotted below.

### Figure 3. Preload dependence of myocardial stiffness

Systolic ( $\square$ ) and diastolic ( $\bullet$ ) myocardial stiffness of a rat heart as a function of LV pressure. \* indicates  $p < 0.01$  vs. initial state.

### Figure 4. $\text{Ca}^{2+}$ dependence of myocardial stiffness

Myocardial stiffness (mean  $\pm$  s.d., N=6) is shown in systole (white background) and diastole (gray background) as a function of  $\text{Ca}^{2+}$  concentration. For each concentration, acquisitions were performed using three different LV volumes. ns indicates  $p =$  non-significant and \* indicates  $p < 0.002$  for the systolic stiffness between states with different  $\text{Ca}^{2+}$ .  $p =$  non significant for the diastolic stiffness both between  $\text{Ca}^{2+}$  concentrations and LV volume (n=6).

**Figure 5. Response to isoproterenol stimulation**

Myocardial stiffness during isoproterenol ( $10^{-7}$  M) stimulation of a rat heart. Isoproterenol was injected at  $t=0$  s.

**Figure 6. Increasing concentrations of isoproterenol**

Systolic stiffness and  $\max(dP/dt)$  for different isoproterenol concentrations ( $10^{-9}$  to  $10^{-7}$  M) acquired 2 minutes after application of the drug. \* indicates  $p<0.05$  and  $\dagger p<0.002$  vs. initial state ( $n=6$ ).

**Figure 7. Correlation between systolic stiffness and systolic pressure used as LV contractility index for one rat heart during the transitory response to isoproterenol stimulation.**

## Tables

**Table 1. Dependence of myocardial stiffness with pressure (mean  $\pm$  s.d).**

	n	Deflated balloon	Balloon inflated at max Systolic Pressure	p-value
Diastolic pressure (mmHg)	6	5.8 $\pm$ 0.7	20.5 $\pm$ 6.9	0.00041
Systolic pressure (mmHg)	6	72 $\pm$ 7.4	124.7 $\pm$ 13.5	0.0001
Diastolic stiffness (kPa)	6	1.7 $\pm$ 0.8	1.8 $\pm$ 0.6	Non-significant
Systolic stiffness (kPa)	6	8.6 $\pm$ 0.7	10.9 $\pm$ 1.1	0.0015

**Table 2. Linear regression between systolic stiffness and systolic pressure.**

	Heart 1	Heart 2	Heart 3	Heart 4	Heart 5	Heart 6	Mean $\pm$ s.d
Slope (kPa/mmHg)	0.239	0.213	0.192	0.228	0.202	0.23	0.22 $\pm$ 0.2
intercept (kPa)	-10.5	-8.7	-7.9	-6.7	-9.0	-9.7	-8.8 $\pm$ 1.3
r <sup>2</sup>	0.94	0.96	0.95	0.98	0.95	0.97	0.96 $\pm$ 0.01
p-value	< 0.0001	< 0.0001	< 0.0001	< 0.0001	< 0.0001	< 0.0001	< 0.0001

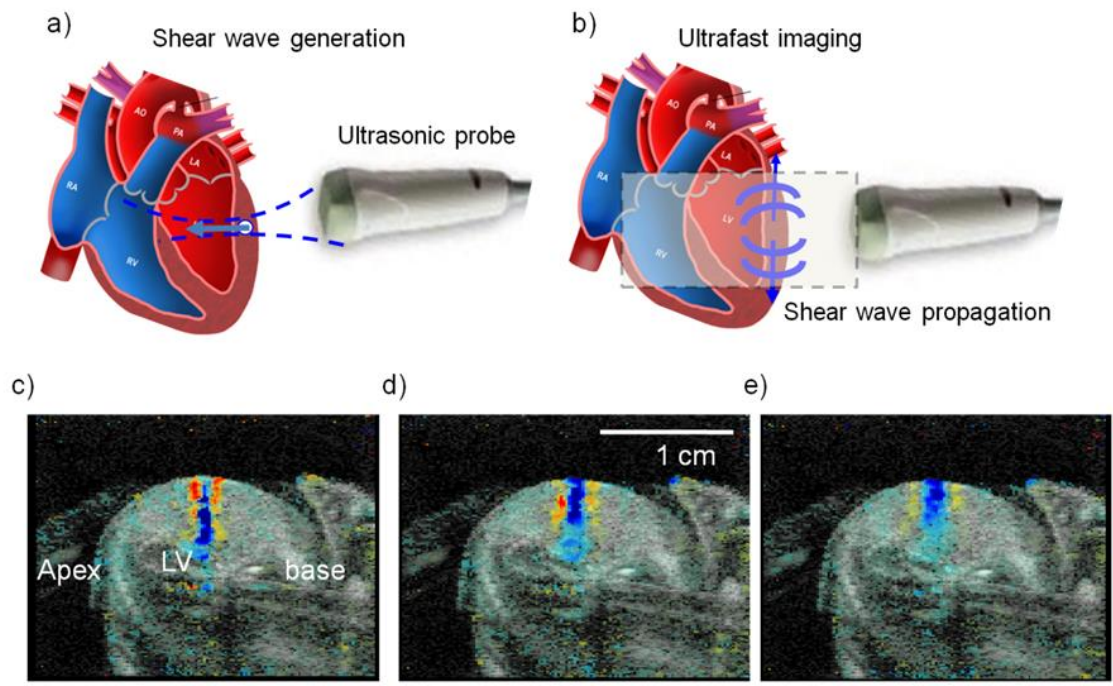


Figure 1

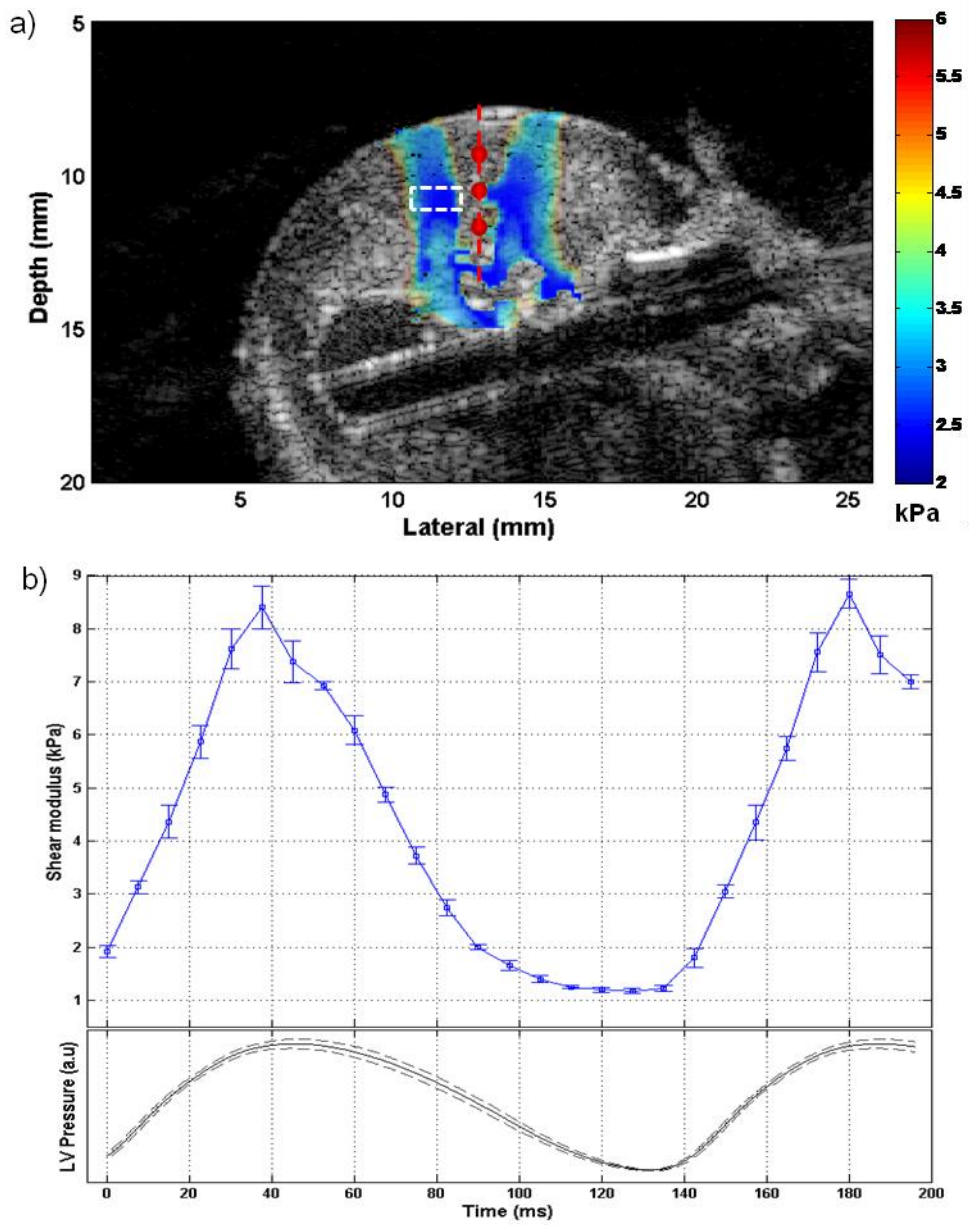


Figure 2

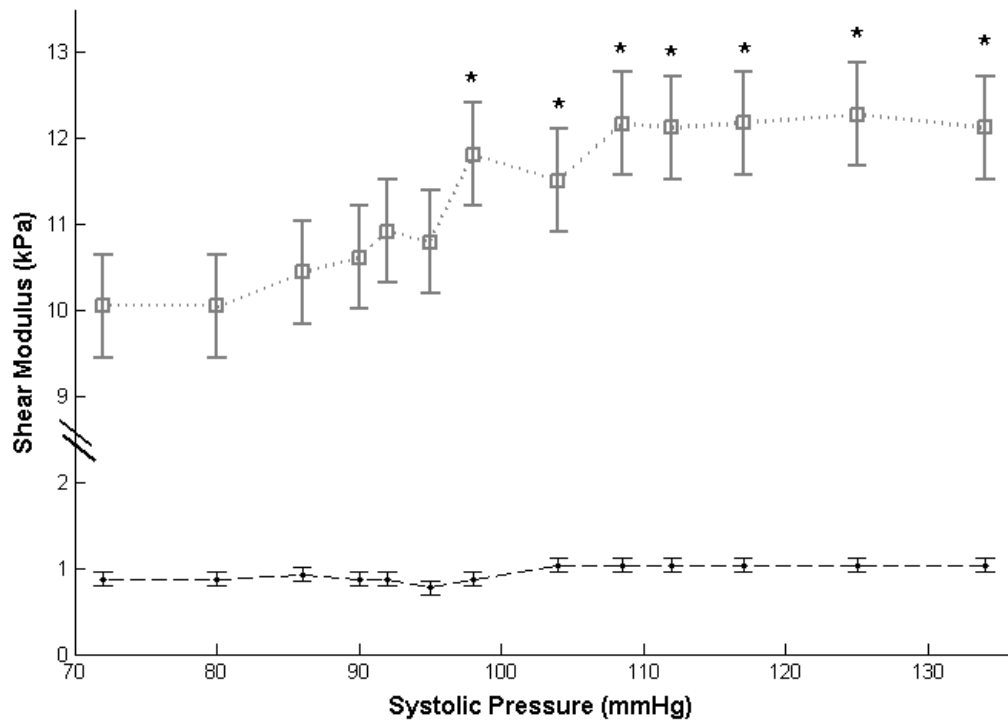


Figure 3

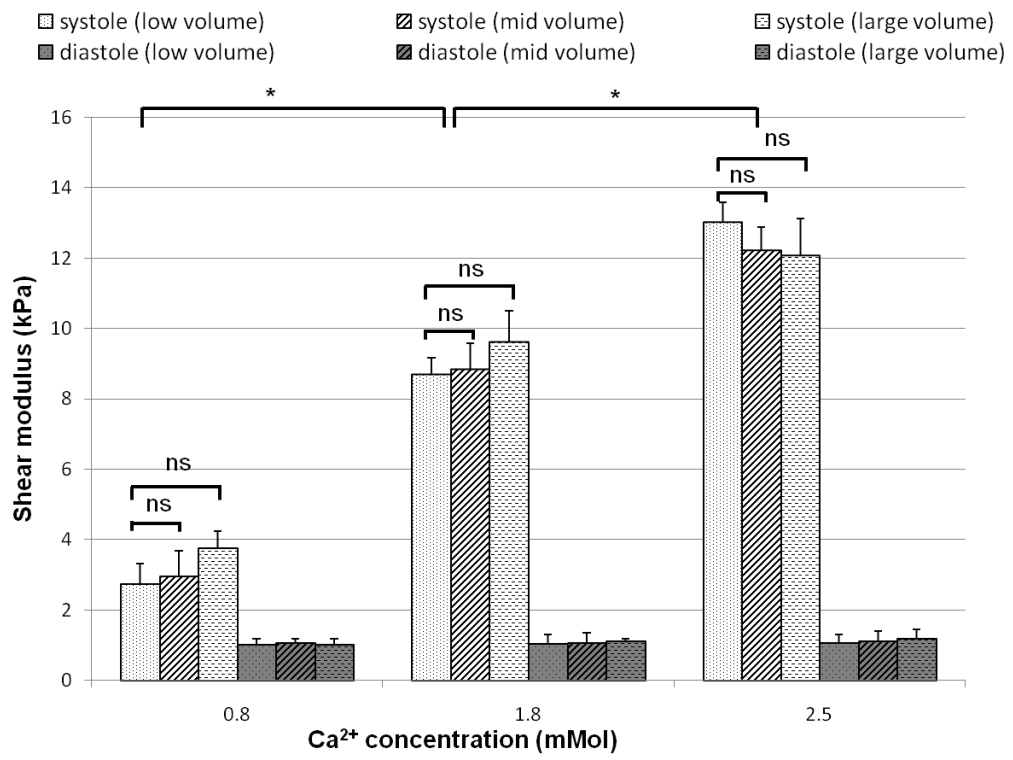


Figure 4

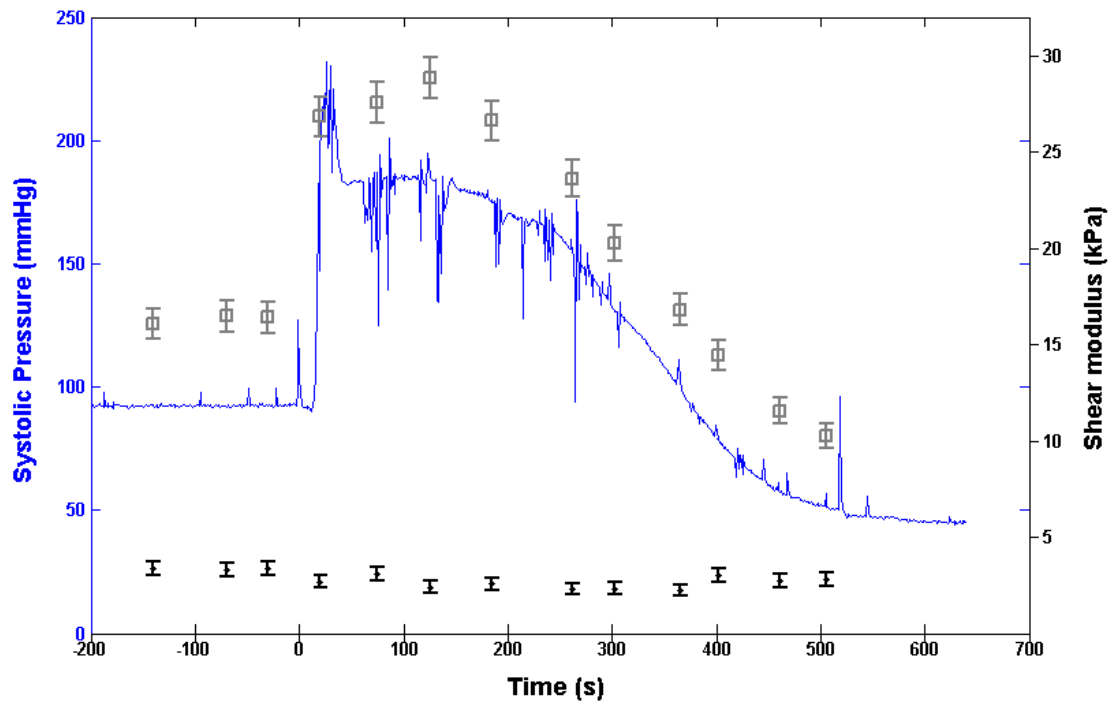


Figure 5

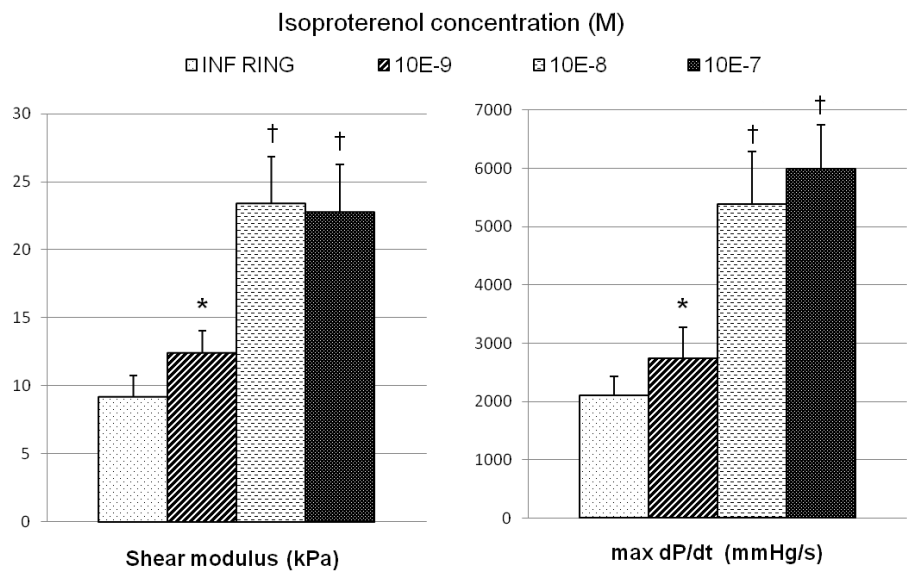


Figure 6

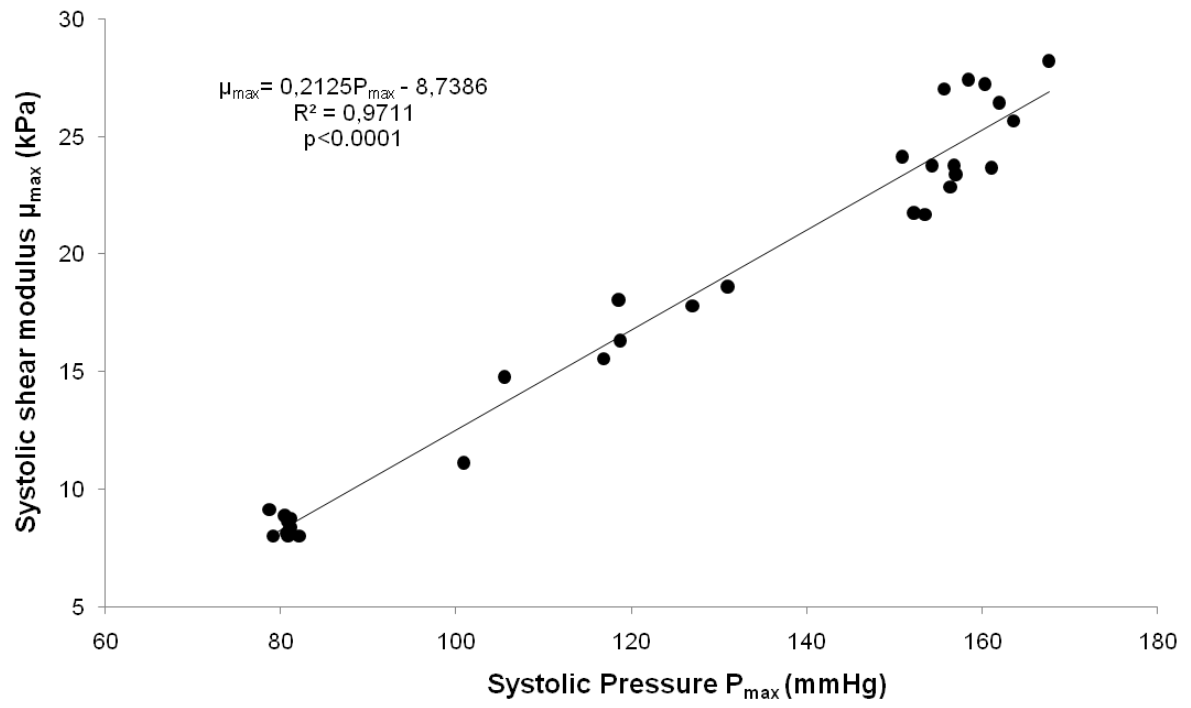


Figure 7